Journal of Volcanology and Geothermal Research 366 (2018) 1–12

Contents lists available at ScienceDirect

Journal of Volcanology and Geothermal Research

journal homepage: www.elsevier.com/locate/jvolgeores

Large-magnitude Pauzhetka caldera-forming eruption in Kamchatka: Astrochronologic age, composition and tephra dispersal

Vera Ponomareva [a,*], Natalia Bubenshchikova [b], Maxim Portnyagin [c,d], Egor Zelenin [e], Alexander Derkachev [f], Sergey Gorbarenko [f], Dieter Garbe-Schönberg [g], Ilya Bindeman [h]

[a] Institute of Volcanology and Seismology, Piip Boulevard 9, Petropavlovsk-Kamchatsky 683006, Russia
[b] Shirshov Institute of Oceanology, 36, Nakhimovsky Prospect, Moscow 117997, Russia
[c] GEOMAR Helmholtz Center for Ocean Research Kiel, Wischhofstrasse 1-3, 24148 Kiel, Germany
[d] V.I. Vernadsky Institute of Geochemistry and Analytical Chemistry, Kosygin St. 19, Moscow 119991, Russia
[e] Geological Institute, Pyzhevsky lane 7, Moscow 119017, Russia
[f] V.I.Il'ichev Pacific Oceanological Institute, Baltiyskaya st., 43, Vladivostok 690041, Russia
[g] Institut für Geowissenschaften, Christian-Albrechts-Universitaet zu Kiel, Ludewig-Meyn-Strasse 10, 24118 Kiel, Germany
[h] Department of Earth Sciences, 1272, University of Oregon, Eugene, OR 97403, USA

ARTICLE INFO

Article history:
Received 17 June 2018
Received in revised form 26 September 2018
Accepted 8 October 2018
Available online 10 October 2018

Keywords:
Tephra
NW Pacific
Kamchatka
Caldera
Glacial termination

ABSTRACT

Correlation of individual tephra layers over large areas permits the assessment of eruption magnitude and synchronization of disparate sedimentary archives. The middle Pleistocene Pauzhetka caldera with a diameter of ~30 km is one of the largest in Kamchatka. Distal tephra from the caldera-forming eruption has, however, never been found, hampering precise estimates of the eruption volume and magnitude. In this paper, we report first geochemical identification of distal tephra from the Pauzhetka caldera in the Northwest (NW) Pacific and Okhotsk Sea sediments recovered by ODP 145 cores 881B, 882A and 884B, and IMAGES cores MD01-2415 and MD01-2416. Distal tephras are rhyolites of narrow compositional range allowing their reliable identification among the studied marine cores using major and trace element data. Geochemical correlation of the distal tephra to the proximal strongly welded and altered ignimbrite was performed based on immobile trace elements determined in situ by laser ablation ICP-MS. Based on this case study, we propose that a number of trace elements (U, Th, Nb, Ta, Zr, Hf, Ti, REE, Y and Sc) are immobile during on-shore alteration of welded tuffs and can be used for correlation of pristine glass and altered rock groundmass allowing direct identification of volcanic source of distal tephra. Our new data on the spatial dispersal of the airborne Pauzhetka tephra in the NW Pacific sediments defines its minimum dense rock equivalent (DRE) volume of ~46 km^3. Together with the exposed volcanic material around the caldera, the total DRE volume is estimated at 150–170 km^3 ($3.8–4.4 \times 10^5$ Mt) corresponding to the eruption magnitude of 7.60–7.65. Stratigraphic position of the Pauzhetka tephra in the studied cores at transition between marine isotope stage 12 and 11c (Termination V) yields a precise astrochronologic age of 421.2 ± 6.6 ka (weighted mean $\pm 2\sigma$), which is 27 ka younger than the published average $^{39}Ar/^{40}Ar$ dates on plagioclase from the proximal ignimbrite. Due to the characteristic composition and precise age, the Pauzhetka tephra may serve as a regional marker for Termination V in the NW Pacific and Okhotsk Sea sediments. A multidisciplinary approach adopted in this study is useful for identification and precise dating of the past explosive eruptions in Kamchatka and other volcanic arcs.

1. Introduction

One of the prerequisites of predicting future giant eruptions is the understanding of size and recurrence intervals of past similar events (e.g., Self and Gertisser, 2015). At the same time, the global record of the large eruptions based mainly on the geological evidence remains incomplete even for the last millennia (Deligne et al., 2010) and deteriorates deeper in time as many eruptions are yet to be identified (Rougier et al., 2016). This is particularly true for remote and highly explosive North Pacific volcanic arcs potentially hazardous for the Northern Hemisphere. One of these arcs is the Kurile-Kamchatka volcanic chain where only Holocene explosive eruptions have been studied in detail (e.g., Braitseva et al., 1995, 1996, 1997, 1998; Bazanova and Pevzner, 2001; Ponomareva et al., 2004, 2013a, 2015; Kyle et al.,

* Corresponding author.
E-mail addresses: vera.ponomareva1@gmail.com (V. Ponomareva), bubenshchikova.nv@ocean.ru (N. Bubenshchikova), mportnyagin@geomar.de (M. Portnyagin), derkachev@poi.dvo.ru (A. Derkachev), gorbarenko@poi.dvo.ru (S. Gorbarenko), dieter.garbe-schoenberg@ifg.uni-kiel.de (D. Garbe-Schönberg), bindeman@uoregon.edu (I. Bindeman).

https://doi.org/10.1016/j.jvolgeores.2018.10.006
0377-0273/

2011) while the Pleistocene record remains obscure and is dotted with only a few dated events (Braitseva et al., 1995; Bindeman et al., 2010; Ponomareva et al., 2013b; Seligman et al., 2014). At the same time, Kamchatka may have the highest concentration of Quaternary calderas per unit of arc length in the world (Hughes and Mahood, 2008), many of which are nested so the number of caldera-forming eruptions is definitely larger than that of the morphologically expressed calderas (e.g., Seligman et al., 2014).

Marine sediments offshore Kamchatka contain numerous tephra layers extensively studied over the last two decades (Cao et al., 1995; Prueher and Rea, 2001; Gorbarenko et al., 2002, 2014; Derkachev et al., 2012a,b; Sakamoto et al., 2005; Derkachev and Portnyagin, 2013). Derkachev et al. (2016) published a detailed account on 23 visible tephra layers in the Pleistocene-Holocene sediments of the Okhotsk Sea, including their composition, age, aerial distribution, and correlation with the oxygen isotope stratigraphy. Furthermore, new geochemical data has been recently published on several tephra layers found in the NW Pacific sediments (Ponomareva et al., 2013a,b, 2015). Despite the high potential for these tephras to provide regional stratigraphic markers, only the 8.4 ka Kurile Lake (KO) and ~30.4 ka Nemo (K_2) layer have been used for core age models up to this point (Gorbarenko et al., 2002).

Many tephras from Ocean Drilling Program (ODP) Leg 145 Sites 881–884 were geochemically characterized by Cao et al. (1995). However, overlapping chemistries did not allow these authors to reliably correlate any of the analyzed tephras between the cores or to particular source volcanoes, thus dispersal and volume of tephra from the large Pleistocene eruptions remained unknown. The difficulties in identification of source volcano arise from a lack of geochemical data on proximal pyroclastic deposits, commonly welded, altered and retaining no volcanic glass, which hampers their direct comparison to glasses from distal tephra and thus assessment of the eruption source, volume and magnitude. The first attempt to date major Kamchatka ignimbrites by $^{40}Ar/^{39}Ar$ geochronology resulted in a dozen of new dates for the most prominent morphologically preserved calderas in Kamchatka (Bindeman et al., 2010). This work has created a dataset to look for products of these large eruptions in the NW Pacific and Okhotsk Sea sediments.

In this paper, we present new geochemical, volumetric and age data on a major explosive eruption in South Kamchatka (NW Pacific), which produced the prominent Pauzhetka caldera (Fig. 1A, B). Geochemical characterization of proximal welded ignimbrite was a challenge due to its strong alteration. However, our new trace element data on the welded ignimbrite groundmass has allowed us to correlate it to a widely spread tephra preserved in ODP 145 cores 881B, 882A and 884B, and IMAGES cores MD01-2415 and MD01-2416, and to estimate volume of the erupted deposits and eruption magnitude. Geochemical correlation of the Pauzhetka tephra in the studied cores allowed us to identify its stratigraphic position at transition between marine isotope stage (MIS) 12 and 11c (Termination V) and estimate its astrochronologic age at 421.2 ± 6.6 ka. A wide spatial dispersal, specific composition, precise age, and unique stratigraphic location within Termination V make the Pauzhetka tephra a prominent isochron linking NW Pacific terrestrial and marine sedimentary archives.

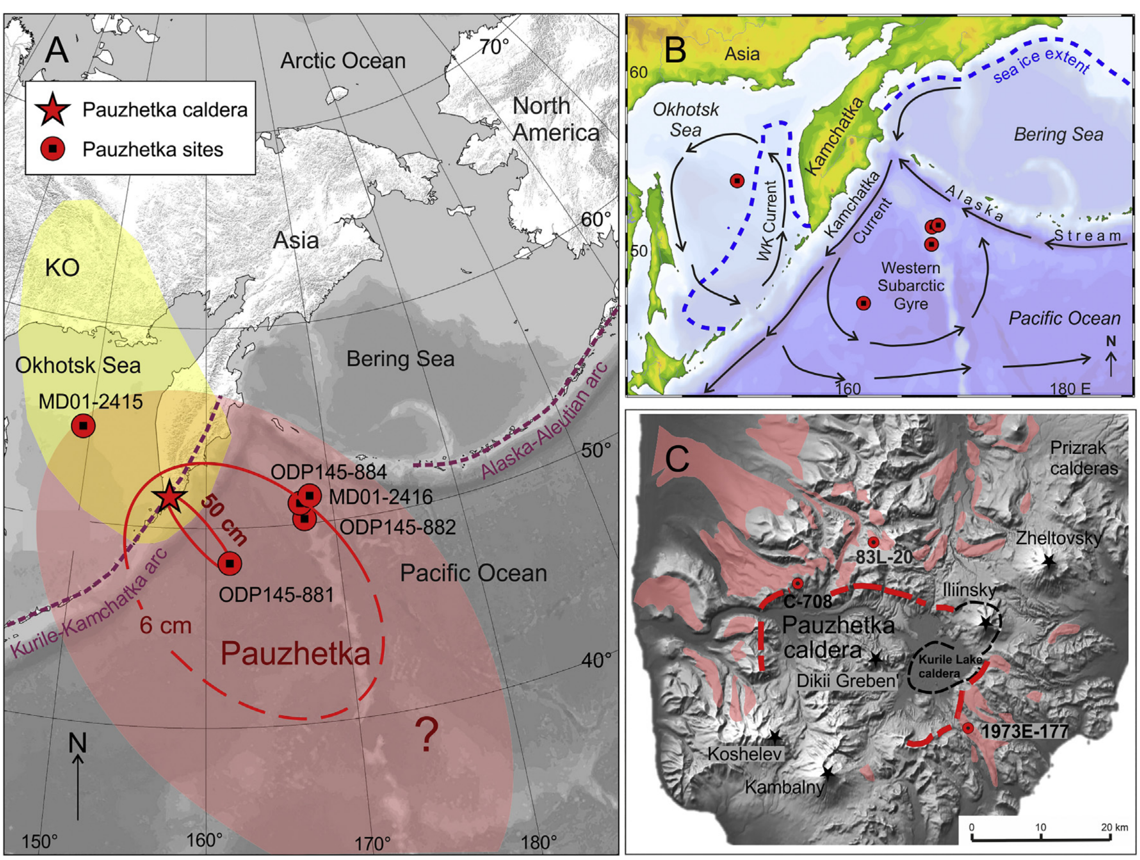

Fig. 1. Location maps for the study area. A. Location of the Pauzhetka caldera and ODP 145 Sites 881, 882 and 884, and IMAGES cores MD01-2415 and MD01-2416. Red outlines show 50 cm and 6 cm isopachs for Pauzhetka tephra (dashed where inferred). Red shading shows presumed Pauzhetka cryptotephra dispersal. Yellow shading provides a dispersal area of the 8.4 ka KO tephra related to the M7 Kurile Lake caldera-forming eruption within the Pauzhetka caldera (Ponomareva et al., 2004). B. Major surface currents (black arrows) and mean annual sea ice extent in winter (blue dashed lines) (Moroshkin, 1966; Rogachev, 2000; Rostov et al., 2002). WK Current = West Kamchatka Current. The map was created with the ODV 4.0 (Schlitzer, 2017). C. The Pauzhetka caldera boundary (in red), remnants of the Golygin welded ignimbrite sheet (red shading), Kurile Lake caldera and pre-Iliinsky collapse crater (black outline; Ponomareva et al., 2004, 2006). Active volcanoes are shown with black stars. Location of $^{40}Ar/^{39}Ar$-dated samples of welded tuff is shown with red circles (Bindeman et al., 2010; Electronic Supplement Table S1). (For interpretation of the references to color in this figure legend, the reader is referred to the web version of this article.)

2. Pauzhetka caldera

The 27 × 18 km Pauzhetka caldera is located in the southernmost part of Kamchatka and hosts two active volcanoes (Iliinsky and Dikii Greben') and the ~8.4 ka Kurile Lake caldera (Fig. 1C; Ponomareva et al., 2004). Caldera rim is well expressed in the west, north and southeast, and is obscured by younger deposits in the south and northeast. The Pauzhetka caldera is surrounded by eroded remnants of once extensive ignimbrite sheet ("Golygin ignimbrite"), which is the only known product of a major caldera-forming eruption (Fig. 1C; Melekestsev, 1980; Erlich, 1986). Golygin ignimbrite is strongly welded. Three $^{40}Ar/^{39}Ar$ dates on plagioclases sampled from different lobes of the extra-caldera ignimbrite suggested the eruption age of 448 ± 20 ka (2σ weighted mean based on the original dates by Bindeman et al., 2010). Total magma volume for this eruption was estimated at 200 km^3 based on the evaluation of published data on the extra- and intra-caldera ignimbrite volumes, and addition of the same volume of airborne ash (Bindeman et al., 2010). However, airfall tephra from the Pauzhetka eruption has never been identified and its dispersal and volume remained unknown.

Only a few later explosive eruptions within the Pauzhetka caldera have been identified: the ~8.4 ka Kurile Lake caldera-forming eruption, and Holocene activity from Iliinsky and Dikii Greben' volcanoes (Bindeman and Bailey, 1994; Ponomareva et al., 2001, 2004, 2006). In addition, a late Pleistocene proto-Kurile Lake caldera eruption was suggested in the eastern part of the Pauzhetka caldera (Melekestsev et al., 1974, 1991) but its products have never been identified.

3. Materials and methods

3.1. Samples

3.1.1. Distal tephra in marine cores

In the course of our research on the largest Kurile-Kamchatka explosive eruptions (Ponomareva et al., 2016) we have sampled and geochemically analyzed Pliocene-Pleistocene tephra from five marine sedimentary cores located 550–670 km west, east and southeast of Kamchatka (Fig. 1A; Electronic Supplement Table S1). Sites 881, 882 and 884 (for those we studied cores 881B, 882A and 884B) were drilled in the NW Pacific during ODP Leg 145 of the R/V JOIDES Resolution in 1992 (Rea et al., 1993). Core MD01-2415 was recovered in the Okhotsk Sea and core MD01-2416 in the NW Pacific during WEPAMA cruise of the R/V Marion Dufresne in 2001 in the frames of IMAGES program (Holbourn et al., 2002). Among the NW Pacific cores, Site 881 is positioned on the abyssal plain, and Sites 882 and 884 and core MD01-2416 are on the Detroit Seamount of the Emperor Seamount Chain (Fig. 1A, B). Core MD01-2415 is located on the northern continental slope of the Okhotsk Sea (Fig. 1A, B).

The most prominent tephra within the MIS 12-11c interval (478–395 ka; Lisiecki and Raymo, 2005), which encompasses the $^{40}Ar/^{39}Ar$ age of the Pauzhetka eruption (448 ± 20 ka, Bindeman et al., 2010) was geochemically correlated between the cores (see Section 4.1) and provisionally identified as belonging to the Pauzhetka caldera-forming eruption. In the NW Pacific cores, samples were taken from a visible tephra layer in cores 881B (Fig. 2), 882A and 884B, and from a sediment layer enriched in tephra pods in core MD01-2416 (Figs. 3 and 4). The tephra layer is 4 to 8.5 cm thick in three cores from the Detroit Seamount and 50 cm thick in core 881B from the abyssal plain (Fig. 1A; Electronic Supplement Table S1). The tephra is represented by fine-grained ash with a typical size of particles of 50–100 μm. The particles are predominantly elongated fragments of bubble walls and their triple junctions, more rarely pumiceous fragments (Fig. 5A, B). In the Okhotsk Sea core MD01-2415, samples were collected from a glass concentration zone (cryptotephra) between 2306 and 2313 cm with a major peak at 2312–2313 cm recognized during count of ice-rafted detritus (IRD) in the >125 μm sediment fraction (Figs. 3 and 4; Bubenshchikova et al., 2015).

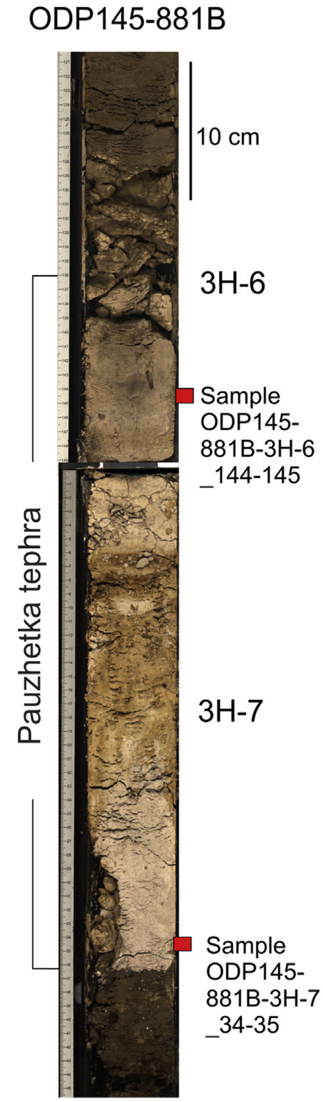

Fig. 2. Pauzhetka tephra in the Northwest Pacific core 881B southeast from Kamchatka. The tephra is present in two adjacent core sections 3H-6 and 3H-7: a massive ash deposit exhibits some changes in color but no admixture of sediments or compositionally different glasses throughout the layer. Geochemically analyzed tephra samples are shown with red squares. (For interpretation of the references to color in this figure legend, the reader is referred to the web version of this article.)

3.1.2. Proximal deposits

In order to geochemically characterize proximal pyroclastic deposits associated with the Pauzhetka caldera-forming eruption and to correlate them with tephra in the studied marine cores, we used two of three $^{40}Ar/^{39}Ar$-dated samples from the opposite lobes of the Golygin welded tuff: C-708 (436 ± 56 ka), and 1973E-177 (441 ± 72 ka) (Fig. 1C; Electronic Supplement Table S1; Bindeman et al., 2010). The samples are quartz-plagioclase-phyric welded tuffs with devitrified glass matrix (Fig. 5C).

3.2. Electron microprobe analysis (EMPA)

Volcanic glasses from tephras and groundmass phases in sample of welded tuff were analyzed at GEOMAR (Kiel, Germany) using JEOL JXA 8200 electron microprobe equipped with five wavelength dispersive spectrometers including 3 high-sensitivity analyzer crystals (2

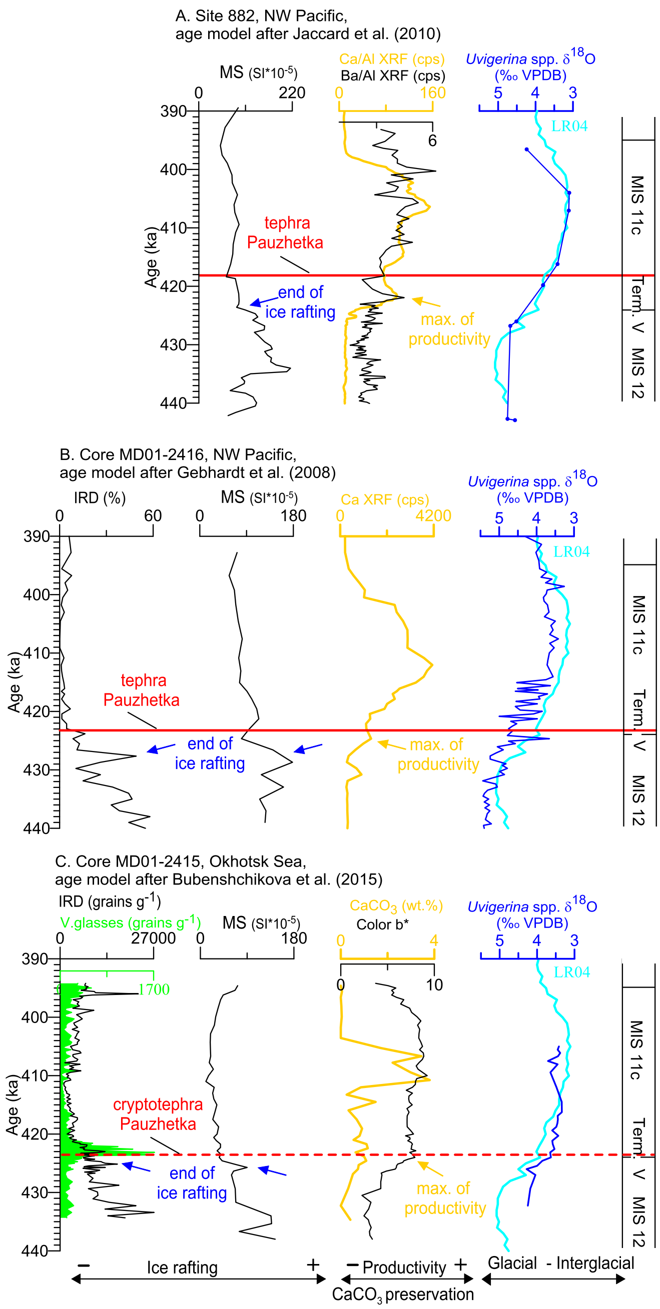

Fig. 3. Position of Pauzhetka tephra against paleoceanological proxies for transition from marine isotope stage (MIS) 12 to 11c. Red solid and dashed lines mark the tephra ages defined for the bottom depths of the tephra layers (Table 1). Note, that data on one of two equivalent age models are presented for core MD01-2416. The LR04 benthic $\delta^{18}O$ stack (light blue) is after Lisiecki and Raymo (2005). A. Site 882. The magnetic susceptibility (MS), Ca/Al XRF (pale), Ba/Al XRF (black) and *Uvigerina* spp. $\delta^{18}O$ (dark blue) data are compiled from cores 882A and 882B after Rea et al. (1993), Haug et al. (1995) and Jaccard et al. (2010). Composite depth and age models are after Tiedemann and Haug (1995) and Jaccard et al. (2010). B. Core MD01-2416. The relative abundance of ice rafted debris (IRD) in >150-μm fraction, MS, Ca XRF (pale) and *Uvigerina* spp. $\delta^{18}O$ (dark blue) data are after Bassinot and Waelbroeck (2002) and Gebhardt et al. (2008). Age model is after Gebhardt et al. (2008). C. Core MD01-2415. The absolute abundances of volcanic glasses (green area) and IRD (black) in >125 μm fraction, MS, $CaCO_3$ (pale), color b* (black), *Uvigerina* spp. $\delta^{18}O$ (dark blue) data are after Bassinot and Waelbroeck (2002) and Bubenshchikova et al. (2015). Age model is after Bubenshchikova et al. (2015). Term V = Termination V. (For interpretation of the references to color in this figure legend, the reader is referred to the web version of this article.)

PETH and TAPH). The analytical conditions for glasses were 15 kV accelerating voltage, 6 nA current and 5 μm electron beam size. The details of the analytical conditions and data reduction can be found in the electronic supplement to Ponomareva et al. (2017). In total we obtained 178 electron microprobe analyses of glasses from 10 tephra samples and 20 analyses of groundmass phases in welded tuff (Electronic Supplement Tables S1, S2, and S5).

3.3. Laser ablation - inductively coupled plasma - mass-spectrometry (LA-ICP-MS) analysis

Trace element analysis by laser ablation-inductively coupled plasma-mass spectrometry (LA-ICP-MS) was performed on two $^{40}Ar/^{39}Ar$ dated samples of Golygin welded tuff (groundmass) and on glasses (single shards) from two tephra samples in cores 881B and 882A (Electronic Supplement Tables S1 and S3). The analyses were performed in the Institute of Geosciences at the Christian-Albrecht University (Kiel, Germany) using a quadrupole ICP-MS Agilent 7900 coupled to a Coherent GeoLasHD ArF 193 nm excimer laser ablation system that was operated with a fluence of 5 $J \cdot cm^{-2}$, a repetition rate of 10 Hz, and 24 μm laser beam diameter. Analyses were performed using a modified large volume ablation cell (Fricker et al., 2011) in a flow of He (0.7 $L \cdot min^{-1}$) with addition of 14 $mL \cdot min^{-1}$ H_2. The carrier gas was mixed with Ar (~1 $L \cdot min^{-1}$) prior to introduction to the ICP-MS. Ten major elements and 31 trace elements were analyzed. Analyses included 20 s background (laser-off) and 30 s signal (laser-on) measurements. Dwell time for different elements varied from 5 to 20 ms depending on their abundance, and one complete measurement cycle lasted 0.607 s. Initial data reduction was performed in GLITTER software (Griffin et al., 2008) that included manual selection of integration windows for background and analytical signal and preliminary calibration. The intensities corrected for background and averaged over the selected intervals were normalized to the intensity of ^{43}Ca isotope and converted to concentrations by matching the sum of 10 element (Si, Ti, Al, Fe, Mn, Mg, Ca, Na, K, P) oxides to 100 wt% (e.g., Kimura and Chang, 2012). The calibration and correction of instrumental drift was based on ATHO-G reference glass (Jochum et al., 2006), which was measured two times after every 18 spots. The data was further filtered for inclusion of phenocryst phases by comparison of major element concentrations with those obtained by EMP and obvious outliers were rejected. BCR2-G, KL2-G and STHS60/8-G glasses (Jochum et al., 2006) were analyzed as unknown (Electronic Supplement Table S3). Based on this data, the analytical precision and accuracy are typically between ±2–8 relative (rel.) % for ca. 20 s long analyses.

LA-ICP-MS data for Na calibrated against ATHO-G glass with recommended Na_2O = 3.75 wt% (Jochum et al., 2006) was found to be systematically offset by ~10 rel. % from the recommended Na values for other reference materials and our EMP data for glass shards with known major element composition. This offset mentioned also by Lowe et al. (2017) suggests that the Na_2O content in ATHO-G glass is likely underestimated. To comply with EMP data, all LA-ICP-MS ATHO-G-calibrated Na concentrations were corrected by a factor of 1.113, which was obtained by fitting data for BCR2-G, KL2-G and STHS60/8-G. This correction has negligible effect (≤0.5 rel. %) on the calculation of concentrations of other elements and was not taken into account.

3.4. Assessment of tephra age in marine cores

Astrochronologic ages of the studied tephra layers were estimated using high-resolution stratigraphic frameworks for Site 882, and cores MD01-2415 and MD01-2416 (Table 1; Galbraith et al., 2008; Gebhardt et al., 2008; Jaccard et al., 2010; Bubenshchikova et al., 2015). For cores 881B and 884B, only low-resolution age models presented in the ODP Leg 145 report were available (Morley et al., 1995; Barron et al., 1995), which provided less precise tephra age estimates (Table 1). For Site 882 we used composite depth-age model based on cores 882A and 882B (Tiedemann and Haug, 1995; Jaccard et al., 2010). The tephra ages were calculated by linear interpolation between tie-points in the core age models. The associated age uncertainties (1σ) were estimated

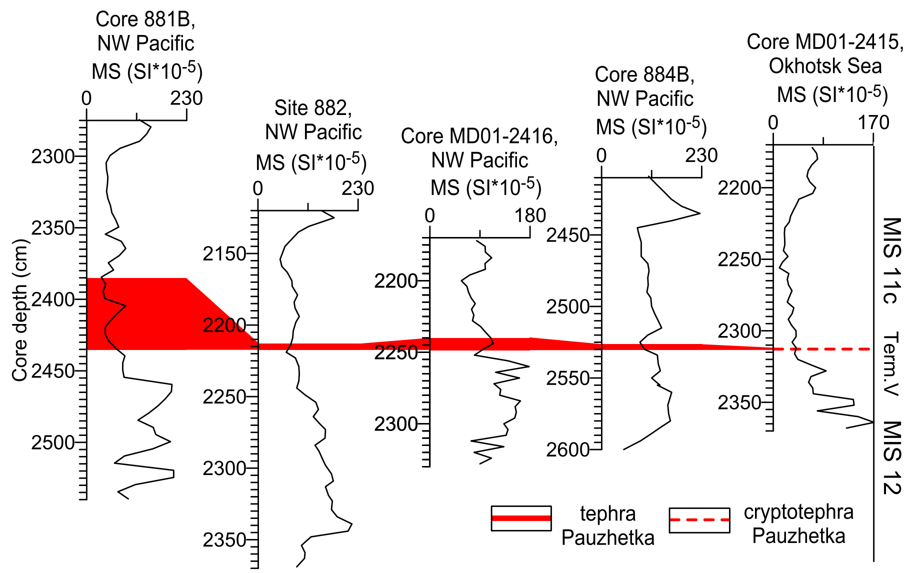

Fig. 4. Position and thickness of Pauzhetka tephra shown together with the core magnetic susceptibility (MS) for transition from marine isotope stage (MIS) 12 to 11c. For cores 881B and 884B, the MS data are after Rea et al. (1993). For cores MD01-2415 and MD01-2416, the MS data are after Bassinot and Waelbroeck (2002). For Site 882, the MS data and composite depths were compiled based on cores 882A and 882B after Rea et al. (1993) and Tiedemann and Haug (1995). Term V = Termination V.

for the ages derived from the high-resolution age models following approach by Govin et al. (2015) (Electronic Supplement Table S4). In order to examine the tephra synchronicity or lead/lag between the cores, we compared paleoceanographic and paleoclimatic conditions at the times of the tephra deposition using published proxy records of Site 882 and cores MD01-2415 and MD01-2416 (Fig. 3) as well as sedimentary magnetic susceptibility (MS) data measured on board and available for all the studied cores (Fig. 4).

4. Results and discussion

4.1. Glass composition

The studied tephra layers were correlated between cores 881B, 882A, 884B and MD01-2416 in the NW Pacific and core MD01-2415 in the Okhotsk Sea (Fig. 1A) based on close similarity of major element compositions of volcanic glasses (Fig. 6; Table 1; Electronic Supplement Tables S1–S3). The tephra glasses have slightly variable medium-K rhyolite composition with 77 and 78.5% SiO_2 and a very narrow range of other major and minor elements determined with EMP (Fig. 6). The minor variability of the glass compositions between the cores as well as bottom-to-top variations within the tephra layer in core 881B only marginally exceed the analytical uncertainty and can be explained by natural compositional variability of melts from a large and compositionally slightly heterogeneous magma chamber.

Trace element compositions of the tephra glasses in distant cores 881B and 882A are identical within the analytical uncertainty (Figs. 1 and 7). The mantle-normalized trace element patterns are typical for subduction-related Si-rich melts. Characteristic features of these patterns are: spoon-shaped distribution of rare earth elements (REE) with negative Eu anomaly and overall enrichment of light rare earth elements (LREE) over middle- and heavy rare earth elements (HREE), island-arc source-related high K_n/La_n, Pb_n/Ce_n, Th_n/Nb_n, B_n/La_n, low Nb_n/La_n (subscript n refers to the mantle-normalized concentrations), and mineral fractionation-related low Sr_n/Ce_n (plagioclase control), Pn/Sm_n (apatite control), Ti_n/Gd_n (magnetite and ilmenite control) ratios.

Based on close resemblance of major and trace element compositions of tephra glasses in all the studied cores and close age estimates for the tephra layers (Table 1; see Section 4.2) we suggest that all the layers represent the same tephra and likely originate from the same volcanic eruption. The tephra dispersal in the NW Pacific sediments (Fig. 1A) indicates its source within South Kamchatka so the studied tephra layers seem to be a likely distal counterpart for the Pauzhetka erupted products.

Unfortunately, our attempts to match the distal tephra to the pyroclastic deposits near the Pauzhetka caldera with the help of microprobe glass analysis failed for a lack of fresh glass in Golygin welded ignimbrite. The latter is composed of large phenocrysts of quartz and plagioclase and accessory pyroxenes, Fe-Ti-oxides, apatite and zircon placed in massive to slightly porous groundmass (Fig. 5C). The groundmass has cryptocrystalline texture composed by microcrystals of magnetite and non-stoichiometric phases with compositions trending toward quartz, K-feldspar, and plagioclase, which are interpreted to be the products of glass alteration (devitrification) in the initially glassy tuff (Electronic Supplement Table S5).

EMP data for devitrified glass shows a very strong compositional heterogeneity on a micron scale (Fig. 8, Electronic Supplement Table S5), which does not permit using this data for reliable comparison with fresh glasses from tephras in marine cores. LA-ICP-MS major element data is less scattered as it represents an average composition for volume of an order of magnitude larger compared to EMPA (~1000 μm^3 for 24 μm laser spot vs. ~80 μm^3 for 6 μm EMP spot). The LA-ICP-MS data plots closer to the anticipated Pauzhetka glass, partly overlaps with the glass compositions but shows larger variability.

Trace element concentrations and their relative variability in devitrified groundmass of welded Golygin ignimbrite are shown in Fig. 9. Alkali (Li, K, Rb, Cs), alkali earth elements (Ba, Sr), B, Eu and V exhibit large variability ($=100\% \times 2\sigma$/Mean), exceeding 40% and suggesting significant mobility of these elements during glass alteration and redistribution between different secondary mineral phases. Variations of alkalis and alkali earths are likely related to their redistribution between secondary plagioclase depleted in K and Rb and enriched in Sr, Eu, Ba and K-feldspar, in contrast to plagioclase, enriched in K and Rb and depleted in Sr, Ba and Eu. Large variations of V content can be explained by entrapment of variable amount of V-rich magnetite. The other 24 trace elements analyzed (U, Th, Nb, Ta, Zr, Hf, Ti, REE, Y and Sc) exhibit a relatively small variability not exceeding 40% even for the least abundant elements (Fig. 9B). These elements are considered as immobile during glass alteration. In this work we used the variability of 40% as an empiric threshold value to identify mobile and immobile elements. Additional research is, however, needed to place more robust

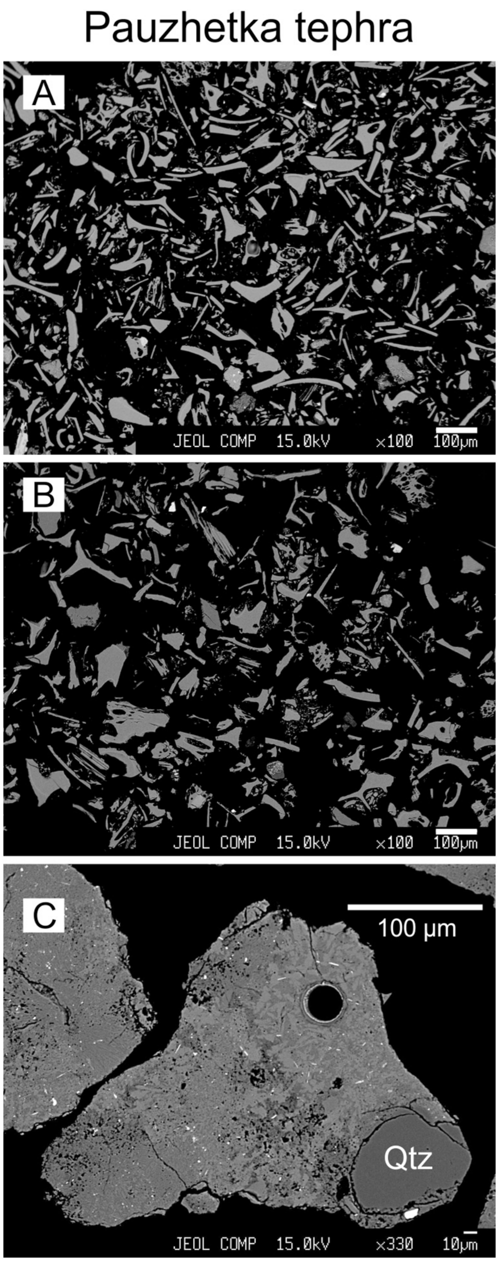

Fig. 5. Back-scattered electron images of polished sections of the Pauzhetka tephra glasses in marine cores and proximal welded tuff embedded in epoxy resin. A, B. Tephra in core 881B and 882A, respectively. C. Golygin welded tuff (sample 1973E-177). Qtz - quartz.

constraints on formal criteria for the element mobility in altered tuffs in subaerial environment. Successful correlation of altered welded ignimbrites using immobile trace elements compositions of bulk samples has been recently reported by Gisbert and Gimeno (2017).

Average concentrations of trace elements in altered glass from welded Golygin ignimbrite are compared to glass compositions in Fig. 7. The data shows a very close resemblance of tuff and tephra glasses in concentrations of immobile elements. Average concentrations of mobile elements in altered glass, except for Li, are also very close to glass composition. This coincidence suggests that the welded tuff alteration was mostly in-situ re-distribution of elements between secondary phases, not an exchange of elements between glass and aqueous fluid that has been well documented for hydrated ignimbrite glasses (e.g., Scott, 1971; Jezek and Noble, 1978). Li depletion observed in altered glass from welded tuff may be related to Li loss during its slow cooling, lithification, and weathering, while Li rich tephra glasses may represent undegassed and rapidly quenched melts (e.g., Hofstra et al., 2013).

In summary, LA-ICP-MS data on concentrations of immobile trace elements suggests that the tephra layers from all the studied cores and Golygin welded tuff belong to the same Pauzhetka eruption.

4.2. Timing of the Pauzhetka caldera-forming eruption

The $^{40}Ar/^{39}Ar$ age of 448 ± 20 ka (weighted mean ± 2σ; Bindeman et al., 2010) for the Pauzhetka eruption falls within a time range of the glacial MIS 12, which duration has been defined from 478 to 424 ka in the LR04 benthic $\delta^{18}O$ record (Lisiecki and Raymo, 2005) (Fig. 10). Differences in the MIS 12 duration between the LR04 time scale and other recent scales, such as the European Project for Ice Coring in Antarctica (EPICA) Dome C (EDC3) and the Antarctic Ice Core Chronology 2012 (AICC2012) are <5 ka that is well within the quoted age uncertainty of 6 ka (Parrenin et al., 2007; Bazin et al., 2013).

Our study of the stratigraphic position, timing and paleoconditions at the time of the Pauzhetka tephra deposition in marine cores indicates a younger eruption age as compared to the mean $^{40}Ar/^{39}Ar$ age. The estimates of tephra age in different cores vary from 418.2 to 446.1 ka (Table 1). Four younger age estimates, which fall into the 418.2 to 423.6 ka range, were derived from the high-resolution age models for Site 882 and cores MD01-2415 and MD01-2416 (Table 1) (Galbraith et al., 2008; Gebhardt et al., 2008; Jaccard et al., 2010; Bubenshchikova et al., 2015). These estimates suggest that the eruption took place during the transition between glacial MIS 12 and interglacial MIS 11c referred to as Termination V, and specifically, during its late stage (Fig. 10). The timing for the Termination V is similar in the LR04, EDC3 and AICC2010 time scales, and the Termination V temporal midpoint is within the 424–426.6 ka range (Lisiecki and Raymo, 2005; Parrenin et al., 2007; Bazin et al., 2013). Close independent age estimate for Termination V (425 ± 5 ka, weighted mean ± 2σ) has been recently provided by Marra et al. (2016) based on the $^{40}Ar/^{39}Ar$ age of a volcanic layer within the San Paolo aggradational succession of the Paleo-Tiber River (Rome, Italy).

In general, a glacial termination is defined between the start and end of the rapid decrease in marine $\delta^{18}O$ during transition from glacial to interglacial climate conditions (e.g., Broecker and Van Donk, 1970; Lisiecki and Raymo, 2005). The position of the Pauzhetka tephra layers relatively to the available *Uvigerina* spp. $\delta^{18}O$ records supports the eruption time during the late Termination V (Fig. 3A–C). The tephra age estimates ranging from 418.2 to 423.6 ka are within the calculated age uncertainties (1σ) from 6.1 to 6.8 ka arising mainly from the dating errors of the reference records used for the age models for Site 882 and cores MD01-2415 and MD01-2416 (Table 1; Electronic Supplement Table S4). This suggests the age variations are an artefact of the reference records rather than a result of the asynchronous deposition of the tephra in these cores.

Among the two older tephra age estimates, one - 430.8 ka in core 884B - points to the eruption time close to onset of the Termination V, while the other – 446.1 ka in core 881B - indicates the eruption time during the glacial MIS 12 (Table 1). However, these estimates were derived from the initial low-resolution age models based on diatom and radiolarian biostratigraphy (Table 1; Barron et al., 1995; Morley et al., 1995), and therefore are considered as questionable. Moreover, the tephra position relative to the MS records in cores 881B and 884B (Fig. 4) does not support the glacial MIS 12 age of the eruption as shown below.

The comparison of the proxy records of the closely located NW Pacific Site 882 and core MD01-2416 (Fig. 3) (Gebhardt et al., 2008; Jaccard et al., 2010) documents similar paleoceanological conditions at the time of the Pauzhetka tephra deposition. In both cores, the tephra is positioned 3–5 ka after the end of active ice rafting and 1–3 ka after the first notable increase in the marine productivity/$CaCO_3$ preservation as indicated by the IRD and/or MS, Ca/Al, Ba/Al, and Ca XRF data (Fig. 3A,

Table 1
Overview of age estimates for the Pauzhetka tephra based on marine cores.

Deposit	Core	Depth (bottom, cm)	Thickness (cm)	Composite depth (bottom, cm)	Age estimate (ka)	Age uncertainty (1σ, ka)[b]	Age model[c] Method	Age model[c] Period (Ma)	Reference
Tephra	ODP145-881B	2435	50.0	–	446.1	–	Radiolarian events, magnetostratigraphy	0–1	Morley et al. (1995)
Tephra	ODP145-882A	1918.5	6.5	2217[a]	**418.2**[a]	6.7	Initial astronomical calibration of the magnetic susceptibility and density curves; correlation of the XRF Ba/Al curve to the EPICA Dome C (EDC) δD ice record on the EDC3 time scale (Jouzel et al., 2007)	0–0.8	Tiedemann and Haug (1995) and Jaccard et al. (2010)
Tephra	ODP145-884B	2530	4.0	–	430.8	–	Radiolarian and diatom events, magnetostratigraphy	0–16	Barron et al. (1995)
Tephra	MD01-2416	2248.5	8.5	–	**423.2**	6.1	Magnetostratigraphy, correlation of the benthic $\delta^{18}O$ curve to the planktic $\delta^{18}O$ stack (Bassinot et al., 1994)	0–1.28	Gebhardt et al. (2008)
					419.2	6.7	Correlation of the XRF Ca curve to the XRF Ca/Ti record of Site 882, having the EDC-based ages (Jouzel et al., 2007)	0–0.5	Galbraith et al. (2008)
Crypto-tephra	MD01-2415	2313	–	–	**423.6**	6.8	Initial astronomical calibration of the color b* record; correlation of the color b* and benthic $\delta^{18}O$ curve to the LR04 stack (Lisiecki and Raymo, 2005)	0.39–0.44	Nürnberg and Tiedemann (2004) and Bubenshchikova et al. (2015)

Note: The age estimates accepted in this study are provided in bold.
[a] Based on the composite age-depth models for ODP145 Site 882 (Tiedemann and Haug, 1995; Jaccard et al., 2010).
[b] Calculations presented in the Electronic Supplement Table S4.
[c] Beyond the radiocarbon dating range.

B). In the high-resolution *Uvigerina* spp. $\delta^{18}O$ record of core MD01-2416 (Fig. 3B) (Gebhardt et al., 2008), the tephra correlates with a local increase in the $\delta^{18}O$ values caused likely by a minor cooling during warm late Termination V. The low-resolution *Uvigerina* spp. $\delta^{18}O$ record of Site 882 (Fig. 3A) (Haug et al., 1995) precludes precise correlation although the occurrence of the tephra within the late Termination V is

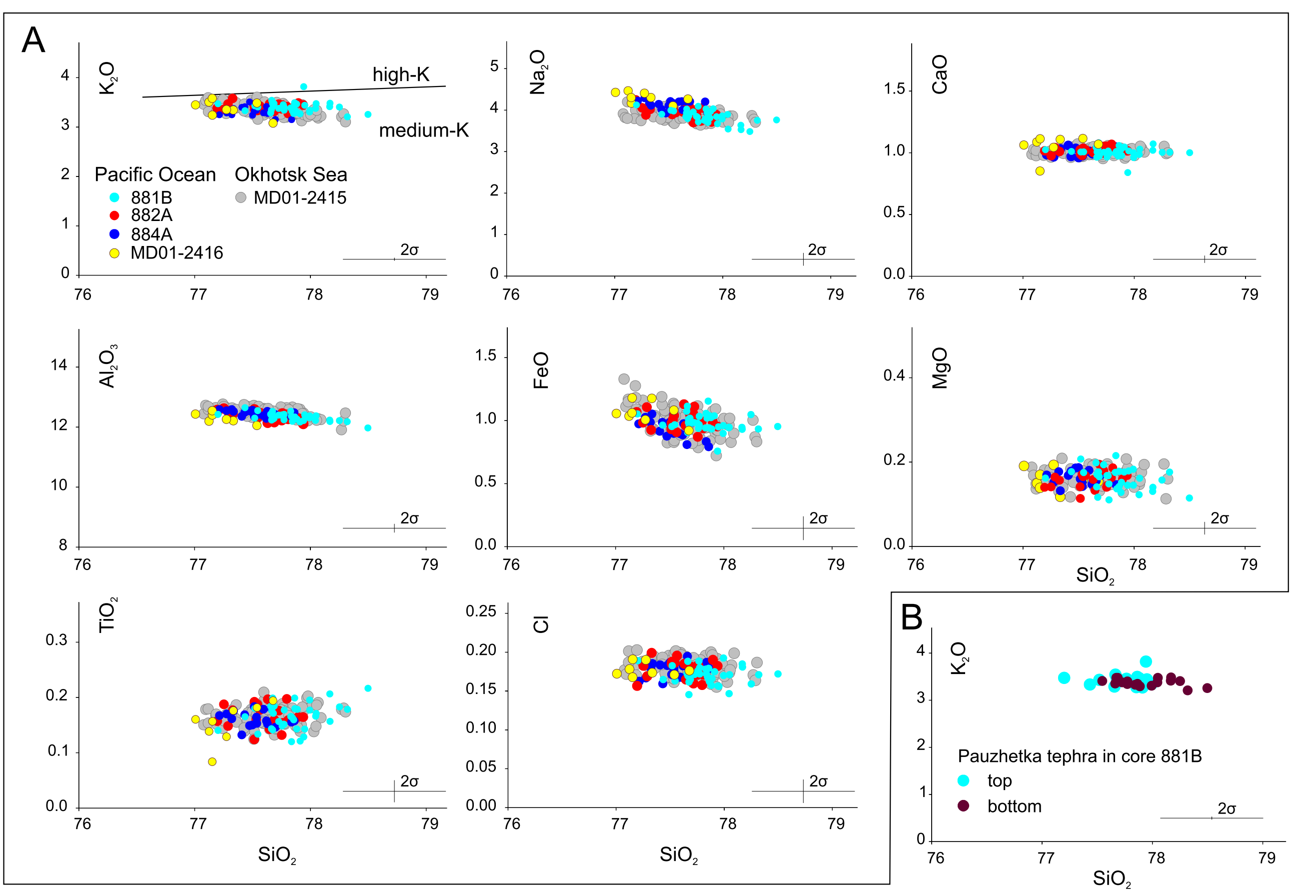

Fig. 6. Composition of the Pauzhetka tephra glasses in marine cores (electron microprobe data) (A), composition of glasses from the bottom and top of the tephra layer in core 881B (B). The fields of medium- and high-K rocks according to Gill (1981). Analytical uncertainty of single points is expressed as 2σ. Oxide concentrations are given in wt%.

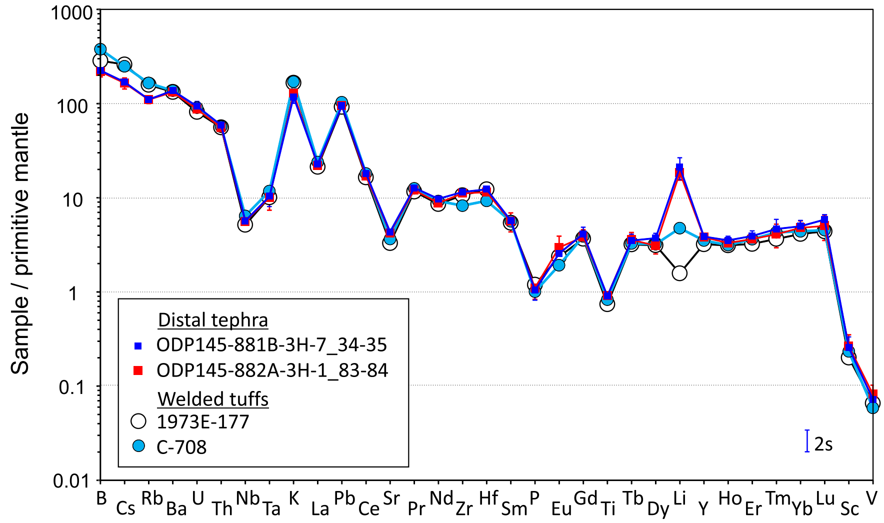

Fig. 7. Comparison of average trace element compositions of the Pauzhetka tephra glasses in cores 881B and 882A and altered groundmass in two samples of Golygin welded ignimbrite (LA-ICP-MS data). Concentrations normalized to primitive mantle values (McDonough and Sun, 1995). Error bars correspond to 2σ.

evident. The results support the synchronous tephra deposition in the NW Pacific Site 882 and core MD01-2416 and preclude significant redeposition by ice rafting.

In the Okhotsk Sea core MD01-2415, the major peak of the Pauzhetka cryptotephra at 423.6 ka occurs 2 ka after the end of active ice rafting and 0.5–1 ka after the first notable increase in the marine productivity/$CaCO_3$ preservation as evidenced from the IRD, MS, $CaCO_3$ (wt%) and color b* data (Fig. 3C). It implies that the paleoceanological conditions at the time of the cryptotephra deposition in the Okhotsk Sea were close to those of the tephra deposition in the NW Pacific (Fig. 3A–C). At the same time, the secondary cryptotephra peak in core MD01-2415 at 423 to 421.5 ka correlates with the last small IRD increase recorded in the IRD curve only (Fig. 3C). It may indicate that the final cease of active sea ice rafting on the northern slope of the Okhotsk Sea occurred a few ka later than in the NW Pacific, and that the sea ice played a role in redeposition of some Pauzhetka glasses into younger sediments. The *Uvigerina* spp. $\delta^{18}O$ record of core MD01-2415 (Fig. 3C) indicates that the cryptotephra occurs during the late Termination V although the record is incomplete for more detailed correlation. Instead, the composition of the benthic foraminiferal assemblage during the MIS12-11c in core MD01-2415 (Bubenshchikova et al., 2015) shows occurrence of the Pauzhetka cryptotephra at 423.6 ka coinciding with a minor cooling during the late Termination V.

Our further analysis of the position of the Pauzhetka tephra layers relative to the MS curves (Fig. 4) provides additional evidence of simultaneous tephra deposition in all the studied cores. In general, the MS of marine sediments is controlled by variations in the IRD supply and, since the onset of the Northern Hemisphere glaciations at ~2.6 Ma, is characterized by low values during interglacial periods and high values during glacial periods (e.g., Past Interglacials Working Group of PAGES, 2016).

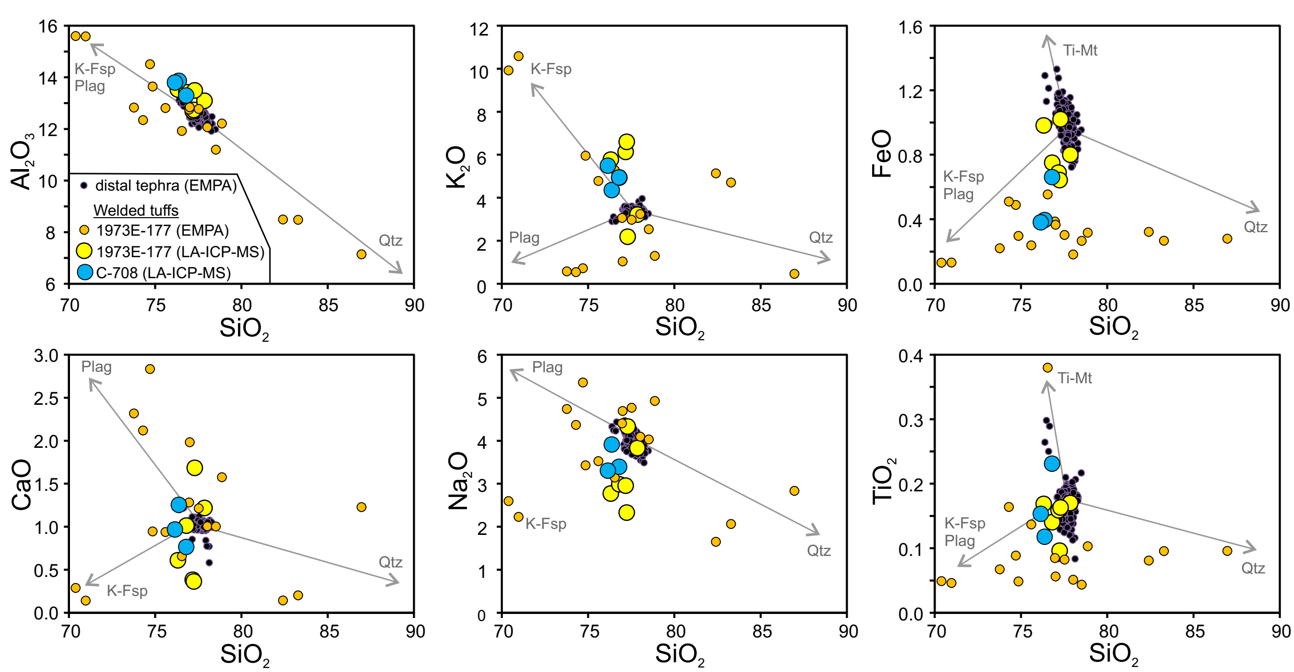

Fig. 8. Comparison of major element compositions of the Pauzhetka tephra glasses in marine cores and altered groundmass in Golygin welded ignimbrite. Arrows indicate mineralogical control of the deviation of single spot analyses of altered groundmass from the average composition of pristine glass. Mineral abbreviations: Plag - plagioclase, K-Fsp – potassium feldspar, Qtz - quartz, Ti-Mag - titanomagnetite. Oxide concentrations are given in wt%.

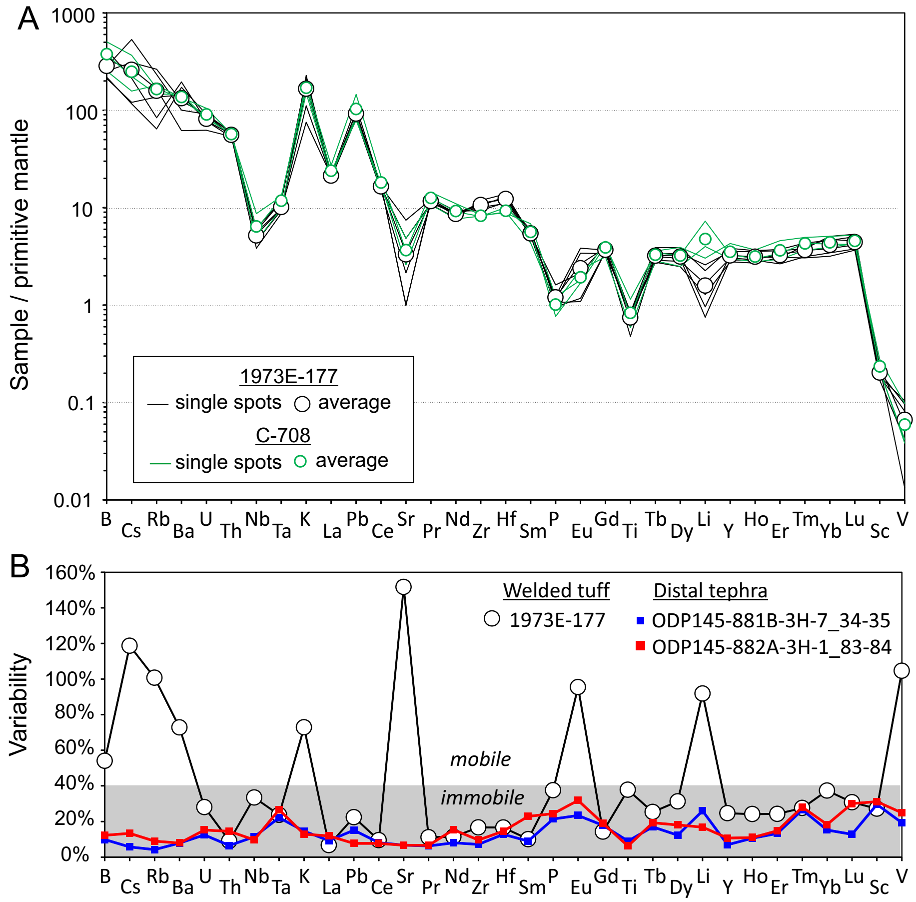

Fig. 9. Trace element heterogeneity of groundmass in Golygin welded ignimbrite. A. Single spot (thin lines) and average (circles) LA-ICP-MS analyses of groundmass in two samples of Golygin welded tuffs. B. Relative variability of trace element concentrations in Golygin welded tuff and in pristine glass from marine cores. Relative variability (V_r) is defined as $V_r =$ Mean/2σ (in %). The elements with $V_r > 40\%$ in the welded tuff are considered as mobile during secondary alteration and should not be used for comparison with glass compositions on the basis of single spot analyses. Average compositions of glass from tephra and groundmass of welded tuff are similar (Fig. 7) and suggest that the secondary alteration of the welded tuff did not result in significant loss or gain of elements, except for Li.

The appearance of the Pauzhetka tephra layer soon after an interval of a rapid decrease in the MS values (Fig. 4) indicates the eruption time during the late Termination V in all the studied cores including core 884B, where the glacial-interglacial variations of the MS are less straightforward. The results also indicate that the glacial age estimates in cores 881B and 884B are not consistent with the actual tephra position beyond the glacial MIS 12 (Table 1 and Fig. 4) and therefore we treat them as unreliable.

Based on the marine core data, we suggest that the Pauzhetka caldera-forming eruption took place within an interval of 418.5–423.6 ka or at 421.2 ± 6.6 ka (weighted mean ± 2σ), which corresponds to the late Termination V (Fig. 10). The discrepancy between the astrochronologic and $^{40}Ar/^{39}Ar$ ages for the Pauzhetka eruption is likely a result of the uncertainties associated with the $^{40}Ar/^{39}Ar$ dating on bulk plagioclase crystals and astrochronologic age models.

The Pauzhetka tephra/cryptotephra can serve as a marker for correlating paleoenvironmental archives among different cores in the NW Pacific and the Okhotsk Sea. It pinpoints a certain short paleoclimate event, specifically a short minor cooling during warm late Termination V (Fig. 3), and permits its tracing through various proxy records. Thus, the Pauzhetka tephra may permit an assessment of synchronicity or lead/lag of climatic shifts between disparate cores that is valuable in the paleoceanographical studies.

4.3. Tephra dispersal and eruption magnitude

The Pauzhetka tephra is expressed as a visible layer only east of the caldera in the NW Pacific cores with the maximum tephra thickness (50 cm) in core 881B, ~600 km south-southeast from the source (Fig. 1A). This core lies beneath the southward flowing branch of the Western Subarctic Gyre (Fig. 1B) that could quickly transport a large amount of tephra from the shelf toward the core location and thus increase a local thickness of the tephra layer. However, in core 881B, the Pauzhetka tephra forms a massive ash layer that exhibits some changes in color but no distinct layering or contamination with the sediment (Fig. 2), which suggests that redeposition of ash within this layer is unlikely. Glasses from the bottom and the top of the tephra layer are compositionally similar but the former have slightly higher SiO_2 contents (Fig. 6B), which is consistent with the “inverted stratigraphy” during typical evacuation of the zoned silicic magma chamber with most evolved material at the onset of a large silicic eruption. Based on the maximum tephra thickness, we suggest that the ashfall axis was directed south-southeast from the source. In the Okhotsk Sea core MD01-2415, located ~560 km west of the caldera (Fig. 1A), the major peak of the Pauzhetka cryptotephra at 423.6 ka might have been also derived from the primary tephra fall, which is assumed from its stratigraphic position and age close to those for the Pauzhetka visible tephra in the NW Pacific cores. Alternatively, it could have originated from syn-eruptive erosion of fresh loose tephra and its redeposition into marine sediments with the help of sea ice and West Kamchatka current.

We have developed a preliminary estimate of Pauzhetka tephra dispersal based on the measured thicknesses in these cores (Fig. 1A). As the mean subduction rate of the Pacific Plate under Kamchatka is ~8 cm/yr (DeMets, 1992), at the time of the eruption the NW Pacific sites were ~34 km farther east from the caldera. This offset is negligible compared

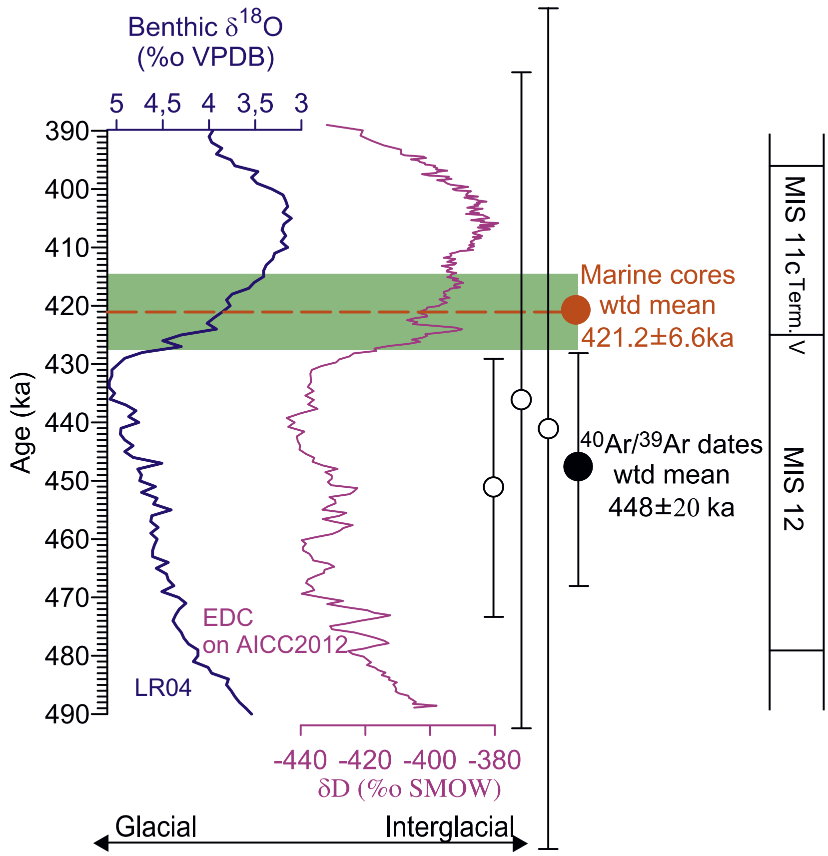

Fig. 10. Comparison of the astrochronologic and $^{40}Ar/^{39}Ar$ age constraints for the Pauzhetka caldera-forming eruption. Weighted mean astrochronologic age is shown with a large red circle and dashed red line; 2σ interval is highlighted in green (Table 1). Weighted mean $^{40}Ar/^{39}Ar$ age is shown with a black circle with a 2σ error bar; individual dates with 2σ error bars from Bindeman et al. (2010) are shown with empty circles. The timing of marine isotope stages (MIS) 12 and 11c and LR04 benthic $\delta^{18}O$ stack (dark blue) is after Lisiecki and Raymo (2005). The EPICA Dome C (EDC) δD ice record on the Antarctic Ice Core Chronology 2012 (AICC2012) time scale (magenta) is after Bazin et al. (2013). Term V = Termination V. (For interpretation of the references to color in this figure legend, the reader is referred to the web version of this article.)

to the dimensions of the isopach area and thus ignored in our assessment. The closely located NW Pacific cores 882A, 884B and MD01-2416 have a mean tephra thickness of 6 cm. These data combined with the 50 cm tephra thickness in core 881B is sufficient to delineate the 50 cm and 6 cm isopachs (Fig. 1A). The cryptotephra found in the Okhotsk Sea core MD01-2415 cannot be used for the isopach map as the thickness of the primary tephra layer is uncertain.

Tephra volume was calculated using the single-segment exponential law (Pyle, 1989) in AshCalc software (Daggitt et al., 2014), which is the most suitable approach in the case when only two isopachs are available. The minimum bulk volume of the Pauzhetka airfall ash comprises 200 km^3, which is consistent with a single-isopach estimate based on the approach by Legros (2000) for each isopach (185 km^3 and 128 km^3 for 50 cm and 6 cm, respectively). The bulk volume of 200 km^3 is close to the minimum estimate and is valid only if core 881B lies exactly on the ash-fall axis, while any offset between the cores and the axis will increase the volume.

The total volume of the Pauzhetka eruptives includes (a) volume of the caldera fill (60–300 km^3, Bindeman et al., 2010, and references therein); (b) volume of the extra-caldera ignimbrite (70–100 km^3, Bindeman et al., 2010); and (c) volume of the airfall ash. Bindeman et al. (2010) evaluated all available estimates for the caldera fill and extra-caldera ignimbrite volumes and came up with a volume of 130–160 km^3. The airfall ash was arbitrarily assigned the same volume, by quoting examples of the similar arc eruptions elsewhere, which provided the total minimum erupted volume of 260–320 km^3 (Bindeman et al., 2010), corresponding to dense rock equivalent (DRE) volume of 130–160 km^3.

Our estimates of a minimal volume of airfall ash (200 km^3) allow us to increase the minimum total eruptive volume to 330–360 km^3. Adopting the mean welded tuff density of ~2 g/cm^3 (Bindeman et al., 2010), ash density of 0.6 g/cm^3 (e.g., Kutterolf et al., 2008b) and rhyolite density of 2.6 g/cm^3, we obtain the total erupted mass of 3.8–4.4 × 10^5 Mt and DRE volume of 150–170 km^3 (46 km^3 distal tephra and 100–123 km^3 proximal deposits), which corresponds to the eruption magnitude of 7.60–7.65 (Mason et al., 2004). We believe that this is a conservative estimate of the eruption magnitude, which will increase with further identification of Pauzhetka tephra farther south in the NW Pacific sediments. Our estimates make the Pauzhetka caldera-forming eruption the second biggest documented eruption for Kamchatka, after the 1.78 Ma Karymshina caldera (Leonov and Rogozin, 2007; Bindeman et al., 2010).

5. Conclusions

1. A widely spread middle Pleistocene tephra was identified and correlated among ODP 145 cores 881B, 882A and 884B and IMAGES cores MD01-2415 and MD01-2416 located in the Northwest Pacific and Okhotsk Sea based on electron microprobe and LA-ICP-MS data, which suggests a M 7.6 explosive eruption from Kamchatka, the second largest eruption documented in this region. Our estimates of the eruption volume and magnitude are conservative and may increase with identification of tephra farther south in the North Pacific sediments.
2. Identification of the eruption source was possible through the comparison of trace element compositions obtained in tephra glasses from the studied cores and for groundmass of strongly welded and

altered Golygin ignimbrite surrounding the Pauzhetka caldera (South Kamchatka). A large number of trace elements (24), reliably analyzed with LA-ICP-MS, were found to be immobile during the glass alteration in the welded tuff and can be used for the direct comparison with the glasses from distal tephra.

3. Stratigraphic position of the Pauzhetka tephra relative to paleoclimate proxies suggests that the caldera-forming eruption took place at the transition from glacial MIS 12 to interglacial MIS 11c (Termination V) and specifically, during minor cooling within its warm late stage. Based on published high-resolution age models for Site 882 and cores MD01-2415 and MD01-2416, the astrochronologic age of the eruption is estimated within an interval of 418.2–423.6 ka or 421.2 $\pm$ 6.6 ka (weighted mean $\pm$ 2σ), that is 27 ka younger than the average $^{40}Ar/^{39}Ar$ age of 448 $\pm$ 20 ka obtained for the proximal deposits (Bindeman et al., 2010). The reasons for the discrepancy between the astrochronologic and $^{40}Ar/^{39}Ar$ ages have to be further investigated once new single-grain $^{40}Ar/^{39}Ar$ dates on the erupted deposits, high-resolution age models for the NW Pacific marine cores, and independent age constrains for the Termination V become available.
4. The case study of the Pauzhetka eruption demonstrates that the combination of volcanological, paleoceanological and geochemical methods has a great potential to reconstruct the history of explosive volcanism in areas, where long-time record is fragmentary. This approach profits from studies of the tephra deposits preserved in marine sediments downwind of volcanic areas that provides opportunity to estimate precise astrochronologic age, volume and magnitude for eruptions. Verification of potential correlations between the distal tephra layers and proximal deposits is possible by using a large number of major and trace elements or just immobile trace elements to compare compositions of tephra glasses and groundmass in altered welded tuffs. This approach has proved to be effective in Kurile-Kamchatka volcanic arc and is readily applicable in other island-arcs worldwide.

Acknowledgements

This research was supported by the Russian Science Foundation grant #16-17-10035 to V. Ponomareva. Analysis of the core MD01-2416 samples was possible thanks to the RFBR grant #16-05-00127 to S.A. Gorbarenko. The results of Section 4.2 were obtained by N. Bubenshchikova within the frames of the theme No. 0149-2018-0016 at the Shirshov Institute of Oceanology. We acknowledge GEOMAR (Kiel, Germany) funding for the electron microprobe analyses. We thank Mario Thöner and Ulrike Westernströer for their assistance with electron probe and LA-ICP-MS analyses. We are grateful to Dirk Nurnberg for providing us with the opportunity to work of the archive part of cores MD01-2415 and MD01-2416 at GEOMAR. We highly appreciate efficient work of the Gulf Coast Repository (Texas, USA) personnel, in particular, Phil Rumford and Helen Evans, who made our 2016 sampling campaign effortless and highly productive. We thank Michael Sarnthein, Samuel Jaccard and Eric Galbraith who shared with us their data on the age models of core MD01-2416 and ODP 145 Site 882, and Matt Loewen for informal comments on English. Comments from two anonymous reviewers helped us to improve our manuscript.

Appendix A. Supplementary data

Supplementary data to this article can be found online at https://doi.org/10.1016/j.jvolgeores.2018.10.006.

References

Barron, J.A., Basov, I.A., Beaufort, L., Dubuisson, G., Gladenkov, A.Y., Morley, J.J., et al., 1995. Biostratigraphic and magnetostratigraphic summary. In: Rea, D.K., Basov, I.A., Scholl, D.W., Allan, J.F. (Eds.), Proc. ODP, Sci. Results. 145. Ocean Drilling Program, College Station, TX, pp. 559–575. https://doi.org/10.2973/odp.proc.sr.145.145.1995.

Bassinot, F.C., Waelbroeck, C., 2002. Shipboard Scientific Party (2002), IMAGES VII Cruise Report, Les Publications de l'Institut Français pour la Recherche et la Technologie Polaires. Les rapports de campagnes à la mer. 01. l'Inst. Français pour la Rech. et la Technol. Polaires, Plouzane, France (435 pp.).

Bassinot, F.C., Labeyrie, L.D., Vincent, E., Quidelleur, X., Shackleton, N.J., Lancelot, Y., 1994. The astronomical theory of climate and the age of the Brunhes-Matuyama magnetic reversal. Earth Planet. Sci. Lett. 126, 91–108. https://doi.org/10.1016/0012-821X(94)90244-5.

Bazanova, L.I., Pevzner, M.M., 2001. Khangar: one more active volcano in Kamchatka. Trans. Russian Acad. Sci. Earth Sci. 377A, 307–310.

Bazin, L., Landais, A., Lemieux-Dudon, B., Toyé Mahamadou Kele, H., Veres, D., Parrenin, F., et al., 2013. An optimized multi-proxy, multi-site Antarctic ice and gas orbital chronology (AICC2012): 120–800 ka. Clim. Past 9, 1715–1731. https://doi.org/10.5194/cp-9-1715-2013.

Bindeman, I.N., Bailey, J.C., 1994. A model of reverse differentiation at Dikii Greben' Volcano, Kamchatka: progressive basic magma vesiculation in a silicic magma chamber. Contrib. Mineral. Petrol. 117 (3), 263–278. https://doi.org/10.1007/BF00310868.

Bindeman, I.N., Leonov, V.L., Izbekov, P.E., Ponomareva, V.V., Watts, K.E., Shipley, N.K., et al., 2010. Large-volume silicic volcanism in Kamchatka: Ar–Ar and U–Pb ages, isotopic, and geochemical characteristics of major pre-Holocene caldera-forming eruptions. J. Volcanol. Geotherm. Res. 189, 57–80. https://doi.org/10.1016/j.jvolgeores.2009.10.009.

Braitseva, O.A., Melekestsev, I.V., Ponomareva, V.V., Sulerzhitsky, L.D., 1995. The ages of calderas, large explosive craters and active volcanoes in the Kuril-Kamchatka region, Russia. Bull. Volcanol. 57 (6), 383–402. https://doi.org/10.1007/BF00300984.

Braitseva, O.A., Melekestsev, I.V., Ponomareva, V.V., Kirianov, V.Yu., 1996. The caldera-forming eruption of Ksudach volcano about cal. AD 240, the greatest explosive event of our era in Kamchatka. J. Volcanol. Geotherm. Res. 70 (1–2), 49–66. https://doi.org/10.1016/0377-0273(95)00047-X.

Braitseva, O.A., Ponomareva, V.V., Sulerzhitsky, L.D., Melekestsev, I.V., Bailey, J., 1997. Holocene key-marker tephra layers in Kamchatka, Russia. Quat. Res. 47 (2), 125–139. https://doi.org/10.1006/qres.1996.1876.

Braitseva, O.A., Bazanova, L.I., Melekestsev, I.V., Sulerzhitsky, L.D., 1998. Largest Holocene eruptions of Avachinsky volcano, Kamchatka. Volcanol. Seismol. 20, 1–27.

Broecker, W.S., Van Donk, J., 1970. Insolation changes, ice volumes, and O-18 record in deep-sea cores. Rev. Geophys. Space Phys. 8 (1), 169–198. https://doi.org/10.1029/RG008i001p00169.

Bubenshchikova, N., Nürnberg, D., Tiedemann, R., 2015. Variations of Okhotsk Sea oxygen minimum zone: comparison of foraminiferal and sedimentological records for latest MIS 12–11c and latest MIS 2–1. Mar. Micropaleontol. 121, 52–69. https://doi.org/10.1016/j.marmicro.2015.09.004.

Cao, L.-Q., Arculus, R.J., McKelvey, B.C., 1995. Geochemistry and petrology of volcanic ashes recovered from Sites 881 through 884: a temporal record of Kamchatka and Kurile volcanism. In: Rea, D.K., Basov, I.A., Scholl, D.W., Allan, J.F. (Eds.), Proc. ODP, Sci. Results. 145. Ocean Drilling Program, College Station, TX, pp. 345–381. https://doi.org/10.2973/odp.proc.sr.145.126.1995.

Daggitt, M.L., Mather, T.A., Pyle, D.M., Page, S., 2014. AshCalc–a new tool for the comparison of the exponential, power-law and Weibull models of tephra deposition. J. Appl. Volcanol. 3 (1), 7. https://doi.org/10.1186/2191-5040-3-7.

Deligne, N., Coles, S., Sparks, R., 2010. Recurrence rates of large explosive volcanic eruptions. J. Geophys. Res. Solid Earth 115. https://doi.org/10.1029/2009JB006554.

DeMets, C., 1992. Oblique convergence and deformation along the Kuril and Japan trenches. J. Geophys. Res. Solid Earth 97 (B12), 17615–17625. https://doi.org/10.1029/92JB01306.

Derkachev, A.N., Portnyagin, M.V., 2013. Marker tephra layers in the late Quaternary deposits of the Sea of Okhotsk as evidence of catastrophic eruptions in the Nemo caldera complex (Onekotan Island, Kuril Islands). Stratigr. Geol. Correl. 21 (5), 553–571. https://doi.org/10.1134/S0869593813040035.

Derkachev, A.N., Nikolaeva, N.A., Gorbarenko, S.A., Harada, N., Sakamoto, T., Iijima, K., et al., 2012a. Characteristics and ages of tephra layers in the central Okhotsk Sea over the last 350 kyr. Deep-Sea Res. II Top. Stud. Oceanogr. 61, 179–192. https://doi.org/10.1016/j.dsr2.2011.05.015.

Derkachev, A.N., Nikolaeva, N.A., Portnyagin, M., Ponomareva, V., Gorbarenko, S.A., Malakhov, M., et al., 2012b. Tephrostratigraphic investigations of the Late Pleistocene-Holocene deposits in the north-western Pacific Ocean (Okhotsk and Bering Seas). AGU Fall Meeting, San Francisco, USA, December 3–7, 2012. Abstract V43B-2830.

Derkachev, A.N., Nikolaeva, N.A., Gorbarenko, S.A., Portnyagin, M.V., Ponomareva, V.V., Nürnberg, D., et al., 2016. Tephra layers of in the Quaternary deposits of the Sea of Okhotsk: distribution, composition, age and volcanic sources. Quat. Int. 425, 248–272. https://doi.org/10.1016/j.quaint.2016.07.004.

Erlich, E., 1986. Geology of the calderas of Kamchatka and Kurile islands with comparison to calderas of Japan and the Aleutians, Alaska. USGS Open File Report 86–291 (300 pp.).

Fricker, M.B., Kutscher, D., Aeschlimann, B., Frommer, J., Dietiker, R., Bettmer, J., et al., 2011. High spatial resolution trace element analysis by LA-ICP-MS using a novel ablation cell for multiple or large samples. Int. J. Mass Spectrom. 307 (1–3), 39–45. https://doi.org/10.1016/j.ijms.2011.01.008.

Galbraith, E.D., Kienast, M., Jaccard, S.L., Pedersen, T.F., Brunelle, B.G., Sigman, D.M., et al., 2008. Consistent relationship between global climate and surface nitrate utilization in the western Subarctic Pacific throughout the last 500 ky. Paleoceanography, 23 https://doi.org/10.1029/2007PA001518.

Gebhardt, H., Sarnthein, M., Grootes, P.M., Kiefer, T., Kuehn, H., Schmieder, F., et al., 2008. Paleonutrient and productivity records from the subarctic North Pacific for

Pleistocene glacial terminations I to V. Paleoceanography 23, PA4212. https://doi.org/10.1029/2007PA001513.

Gill, J.B., 1981. Orogenic Andesites and Plate Tectonics. Springer, Berlin (390 pp.).

Gisbert, G., Gimeno, D., 2017. Ignimbrite correlation using whole-rock geochemistry: an example from the Sulcis (SW Sardinia, Italy). Geol. Mag. 154 (4), 740–756. https://doi.org/10.1017/S0016756816000327.

Gorbarenko, S.A., Nürnberg, D., Derkachev, A.N., Astakhov, A.S., Southon, J.R., Kaiser, A., 2002. Magnetostratigraphy and tephrochronology of the Upper Quaternary sediments in the Okhotsk Sea: implication of terrigenous, volcanogenic and biogenic matter supply. Mar. Geol. 183 (1–4), 107–129. https://doi.org/10.1016/S0025-3227(02)00164-0.

Gorbarenko, S., Chebykin, E.P., Goldberg, E.L., Stepanova, O.G., Lu, H., 2014. Chronicle of regional volcanic eruptions recorded in Okhotsk Sea sediments over the last 350 ka. Quat. Geochronol. 20, 29–38. https://doi.org/10.1016/j.quageo.2013.10.006.

Govin, A., Capron, E., Tzedakis, P.C., Verheyden, S., Ghaleb, B., Hillaire-Marcel, C., et al., 2015. Sequence of events from the onset to the demise of the Last Interglacial: evaluating strengths and limitations of chronologies used in climatic archives. Quat. Sci. Rev. 129, 1–36. https://doi.org/10.1016/j.quascirev.2015.09.018.

Griffin, W., Powell, W., Pearson, N., O'Reilly, S., 2008. GLITTER: data reduction software for laser ablation ICP-MS. Laser Ablation-ICP-MS in the Earth Sciences Mineralogical Association of Canada Short Course Series 40, pp. 204–207.

Haug, G.H., Maslin, M.A., Sarnthein, M., Stax, R., Tiedemann, R., 1995. Evolution of Northwest Pacific sedimentation patterns since 6 Ma (Site 882). In: Rea, D.K., Basov, I.A., Scholl, D.W., Allan, J.F. (Eds.), Proc. ODP, Sci. Results. 145. Ocean Drilling Program, College Station, TX, pp. 293–314. https://doi.org/10.2973/odp.proc.sr.145.115.1995.

Hofstra, A.H., Todorov, T.I., Mercer, C.N., Adams, D.T., Marsh, E.E., 2013. Silicate melt inclusion evidence for extreme pre-eruptive enrichment and post-eruptive depletion of lithium in silicic volcanic rocks of the western United States: implications for the origin of lithium-rich brines. Econ. Geol. 108 (7), 1691–1701. https://doi.org/10.2113/econgeo.108.7.1691.

Holbourn, A., Kiefer, T., Pflaumann, U., Rothe, S., 2002. WEPAMA Cruise MD 122/IMAGES VII, Rapp. Campagnes Mer OCE/2002/01. Inst. Polaire Fr. Paul Emile Victor (IPEV), Plouzané, France.

Hughes, G.R., Mahood, G.A., 2008. Tectonic controls on the nature of large silicic calderas in volcanic arcs. Geology 36, 627–630. https://doi.org/10.1130/g24796a.1.

Jaccard, S.L., Galbraith, E.D., Sigman, D.M., Haug, G.H., 2010. A pervasive link between Antarctic ice core and subarctic Pacific sediment records over the past 800 kyrs. Quat. Sci. Rev. 29 (1–2), 206–212. https://doi.org/10.1016/j.quascirev.2009.10.007.

Jezek, P.A., Noble, D.C., 1978. Natural hydration and ion-exchange of obsidian - electron-microprobe study. Am. Mineral. 63 (3–4), 266–273.

Jochum, K.P., Stoll, B., Herwig, K., Willbold, M., Hofmann, A.W., Amini, M., et al., 2006. MPI-DING reference glasses for in situ microanalysis: new reference values for element concentrations and isotope ratios. Geochem. Geophys. Geosyst. 7 (2).

Jouzel, J., Masson-Delmotte, V., Cattani, O., Dreyfus, G., Falourd, S., Hoffmann, G., et al., 2007. Orbital and millennial Antarctic climate variability over the past 800 000 years. Science 317, 793–796. https://doi.org/10.1126/science.1141038.

Kimura, J.-I., Chang, Q., 2012. Origin of the suppressed matrix effect for improved analytical performance in determination of major and trace elements in anhydrous silicate samples using 200 nm femtosecond laser ablation sector-field inductively coupled plasma mass spectrometry. J. Anal. At. Spectrom. 27, 1549–1559. https://doi.org/10.1039/C2JA10344C.

Kutterolf, S., Freundt, A., Peréz, W., 2008b. The Pacific offshore record of Plinian arc volcanism in Central America, part 2: tephra volumes and erupted masses. Geochem. Geophys. Geosyst. 9 (2). https://doi.org/10.1029/2007GC001791.

Kyle, Ph.R., Ponomareva, V.V., Rourke Schluep, R., 2011. Geochemical characterization of marker tephra layers from major Holocene eruptions in Kamchatka, Russia. Int. Geol. Rev. 53 (9), 1059–1097. https://doi.org/10.1080/00206810903442162.

Legros, F., 2000. Minimum volume of a tephra fallout deposit estimated from a single isopach. J. Volcanol. Geotherm. Res. 96, 25–32. https://doi.org/10.1016/S0377-0273(99)00135-3.

Leonov, V.L., Rogozin, A.N., 2007. Karymshina, a giant supervolcano caldera in Kamchatka: boundaries, structure, volume of pyroclastics. J. Volcanol. Seismol. 1 (5), 296–309. https://doi.org/10.1134/S0742046307050028.

Lisiecki, L.E., Raymo, M., 2005. A Pliocene–Pleistocene stack of 57 globally distributed benthic ^{18}O records. Paleoceanography 20, PA1003. https://doi.org/10.1029/2004PA001071.

Lowe, D.J., Pearce, N.J., Jorgensen, M.A., Kuehn, S.C., Tryon, C.A., Hayward, C.L., 2017. Correlating tephras and cryptotephras using glass compositional analyses and numerical and statistical methods: review and evaluation. Quat. Sci. Rev. 175, 1–44. https://doi.org/10.1016/j.quascirev.2017.08.003.

Marra, F., Rohling, E.J., Florindo, F., Jicha, B., Nomade, S., Pereira, A., et al., 2016. Independent $^{40}Ar/^{39}Ar$ and ^{14}C age constraints on the last five glacial terminations from the aggradational successions of the Tiber River, Rome (Italy). Earth Planet. Sci. Lett. 449, 105–117. https://doi.org/10.1016/j.epsl.2016.05.037.

Mason, B.G., Pyle, D.M., Oppenheimer, C., 2004. The size and frequency of the largest explosive eruptions on Earth. Bull. Volcanol. 66 (8), 735–748. https://doi.org/10.1007/s00445-004-0355-9.

McDonough, W.F., Sun, S.S., 1995. The composition of the Earth. Chem. Geol. 120 (3–4), 223–253. https://doi.org/10.1016/0009-2541(94)00140-4.

Melekestsev, I.V., 1980. Volcanism and Relief Formation. Nauka, Moscow (in Russian).

Melekestsev, I.V., Braitseva, O.A., Erlich, E.N., Kozhemyaka, N.N., 1974. In: Luchitsky, I.V. (Ed.), Volcanic Mountains and Plains, in Kamchatka, Kurile and Commander Islands. Nauka, Moscow, pp. 162–234 (In Russian).

Melekestsev, I.V., Glushkova, O.Yu., Kirianov, V.Yu., Lozhkin, A.V., Sulerzhitsky, L.D., 1991. Age and origin of Magadan ashes. Trans. (Doklady) Russian Acad. Sci. Earth Sci. Sect. 317 (5), 1188–1192.

Morley, J.J., Tiase, V.L., Ashby, M.M., Kashgarian, M., 1995. A high-resolution stratigraphy from Pleistocene sediments from North Pacific Sites 881, 883, and 887 based on abundance variations of the radiolarian *Cycladophora davisiana*. In: Rea, D.K., Basov, I.A., Scholl, D.W., Allan, J.F. (Eds.), Proc. ODP, Sci. Results. 145. Ocean Drilling Program, College Station, TX, pp. 133–140. https://doi.org/10.2973/odp.proc.sr.145.108.1995.

Moroshkin, K.V., 1966. Water Masses of the Sea of Okhotsk (Vodnie Massi Ohotskogo Moriya). Nauka, Moscow (66 pp. (in Russian)).

Nürnberg, D., Tiedemann, R., 2004. Environmental change in the Sea of Okhotsk during last 1.1 million years. Paleoceanography 19, PA4011. https://doi.org/10.1029/2004Pa001023.

Parrenin, F., Barnola, J.-M., Beer, J., Blunier, T., Castellano, E., Chappellaz, J., et al., 2007. The EDC3 chronology for the EPICA Dome C ice core. Clim. Past 3, 485–497. https://doi.org/10.5194/cp-3-485-2007.

Past Interglacials Working Group of PAGES, 2016. Interglacials of the last 800,000 years. Rev. Geophys. 54. https://doi.org/10.1002/2015RG000482.

Ponomareva, V.V., Sulerzhitsky, L.D., Dirksen, O.V., Zaretskaia, N.E., 2001. Holocene paleosols as records of intervals of volcanic quiescence in the Kurile Lake region, South Kamchatka. In: Juvigne´, E., Raynal, J.P. (Eds.), Tephras, Chronology, Archaeology. Les Dossiers de l'Archéo-Logie. vol. 1. CDERAD Ed., Goudek, pp. 91–100.

Ponomareva, V., Kyle, P., Melekestsev, I., Rinkleff, P., Dirksen, O., Sulerzhitsky, L., et al., 2004. The 7600 (^{14}C) year BP Kurile Lake caldera-forming eruption, Kamchatka, Russia: stratigraphy and field relationships. J. Volcanol. Geotherm. Res. 136 (3), 199–222. https://doi.org/10.1016/j.jvolgeores.2004.05.013.

Ponomareva, V.V., Melekestsev, I.V., Dirksen, O.V., 2006. Sector collapses and large landslides on Late Pleistocene–Holocene volcanoes in Kamchatka, Russia. J. Volcanol. Geotherm. Res. 158 (1–2), 117–138. https://doi.org/10.1016/j.jvolgeores.2006.04.016.

Ponomareva, V., Portnyagin, M., Derkachev, A., Pendea, I.F., Bourgeois, J., Reimer, P.J., et al., 2013a. Early Holocene M ~ 6 explosive eruption from Plosky volcanic massif (Kamchatka) and its tephra as a link between terrestrial and marine paleoenvironmental records. Int. J. Earth Sci. 102 (6), 1673–1699. https://doi.org/10.1007/s00531-013-0898-0.

Ponomareva, V., Portnyagin, M., Derkachev, A., Juschus, O., Garbe-Schönberg, D., Nürnberg, D., 2013b. Identification of a widespread Kamchatkan tephra: a middle Pleistocene tie-point between Arctic and Pacific paleoclimatic records. Geophys. Res. Lett. 40 (14), 3538–3543. https://doi.org/10.1002/grl.50645.

Ponomareva, V., Portnyagin, M., Pevzner, M., Blaauw, M., Kyle, Ph., Derkachev, A., 2015. Tephra from andesitic Shiveluch volcano, Kamchatka, NW Pacific: chronology of explosive eruptions and geochemical fingerprinting of volcanic glass. Int. J. Earth Sci. 104, 1459e1482. https://doi.org/10.1007/s00531-015-1156-4.

Ponomareva, V., Portnyagin, M., Derkachev, A., Bazanova, L., Bubenshchikova, N., Garbe-Schönberg, D., et al., 2016. Building the record of late Miocene to Pleistocene explosive activity in the Kurile-Kamchatka volcanic arc: initial results and challenges. AGU Fall Meeting, San Francisco, December 12–16, Abstract V11A-2762.

Ponomareva, V., Portnyagin, M., Pendea, F., Zelenin, E., Bourgeois, J., Pinegina, T., et al., 2017. A full Holocene tephrochronology for the Kamchatsky Peninsula region: applications from Kamchatka to North America. Quat. Sci. Rev. 168, 101–122. https://doi.org/10.1016/j.quascirev.2017.04.031.

Prueher, L.M., Rea, D.K., 2001. Tephrochronology of the Kamchatka–Kurile and Aleutian arcs: evidence for volcanic episodicity. J. Volcanol. Geotherm. Res. 106 (1–2), 67–84. https://doi.org/10.1016/S0377-0273(00)00266-3.

Pyle, D.M., 1989. The thickness, volume and grainsize of tephra fall deposits. Bull. Volcanol. 51 (1), 1–15. https://doi.org/10.1007/BF01086757.

Rea, D.K., Basov, I.A., Janecek, T.R., Palmer-Julson, A., et al., 1993. Proc. ODP, Init. Repts. 145. Ocean Drilling Program, College Station, TX. https://doi.org/10.2973/odp.proc.ir.145.1993.

Rogachev, K.A., 2000. Recent variability in the Pacific western subarctic boundary currents and Sea of Okhotsk. Prog. Oceanogr. 47 (2–4), 299–336.

Rostov, I.D., Yurasov, G.I., Rudyh, N.I., et al., 2002. Oceanographic Atlas of the Bering Sea, Okhotsk Sea and Japan/East Sea. Information Resources of V.I. Il'ichev Pacific Oceanological Institute, CD–ROM. vol. 2. http://www.pacificinfo.ru/.

Rougier, J., Sparks, S.R., Cashman, K.V., 2016. Global recording rates for large eruptions. J. Appl. Volcanol. 5 (1), 11. https://doi.org/10.1186/s13617-016-0051-4.

Sakamoto, T., Ikehara, M., Aoki, K., Iijima, K., Kimura, N., Nakatsuka, T., et al., 2005. Ice-rafted debris (IRD)-based sea-ice expansion events during the past 100 kyrs in the Okhotsk Sea. Deep-Sea Res. 52, 2275–2301. https://doi.org/10.1016/j.dsr2.2005.08.007.

Schlitzer, R., 2017. Ocean Data View Version 4.0.0. Alfred Wegener Institute, Bremerhaven, Germany http://www.odv.awi.de/.

Scott, R.B., 1971. Alkali exchange during devitrification and hydration of glasses in ignimbrite cooling units. J. Geol. 79 (1), 100–110.

Self, S., Gertisser, R., 2015. Tying down eruption risk. Nat. Geosci. 8, 248–250. https://doi.org/10.1038/ngeo2403.

Seligman, A., Bindeman, I., Jicha, B., Ellis, B., Ponomareva, V., Leonov, V., 2014. Multi-cyclic and isotopically diverse silicic magma generation in an arc volcano: Gorely eruptive center, Kamchatka, Russia. J. Petrol. 55 (8), 1561–1594. https://doi.org/10.1093/petrology/egu034.

Tiedemann, R., Haug, G.H., 1995. Astronomical calibration of cycle stratigraphy for Site 882 in the northwest Pacific. In: Rea, D.K., Basov, I.A., Scholl, D.W., Allan, J.F. (Eds.), Proc. ODP, Sci. Results. 145. Ocean Drilling Program, College Station, TX, pp. 283–292. https://doi.org/10.2973/odp.proc.sr.145.124.1995.